Magnetostructural phase transitions in $La_{1-x}Sr_xMnO_3$ with controlled carrier density

A. Asamitsu, Y. Moritomo, R. Kumai, and Y. Tomioka

Joint Research Center for Atom Technology (JRCAT), Tsukuba 305, Japan

Y. Tokura

Joint Research Center for Atom Technology (JRCAT), Tsukuba 305, Japan
and Department of Applied Physics, University of Tokyo, Tokyo 113, Japan

(Received 2 February 1996)

Magnetic-field-induced structural phase transitions between the orthorhombic and rhombohedral structures have been investigated for single crystals of perovskite-type manganese oxides, $La_{1-x}Sr_xMnO_3$, with finely controlled carrier density ($x = 0.16$–0.18). In $x = 0.170$ crystal, whose composition is tuned so that the structural transition temperature T_S is located close to the Curie temperature T_C, the T_S decreases drastically from 280 K at zero field down to 220 K at 7 T. Such a large magnetostructural effect arises from the mutual coupling among the kinetic energy of doped e_g carriers, the local-spin moment of t_{2g} electrons, and the lattice degree of freedom. We have determined the structural phase diagram in the plane of temperature and magnetic field. For $x = 0.16$ or 0.18 crystals, on the other hand, the T_S's that differ considerably from respective T_C's have not been changed conspicuously up to 7 T. Thermodynamical aspects of the interesting magnetostructural phenomena are argued in terms of the free energy with coupled order parameters, the magnetization M, and the lattice distortion Q. [S0163-1829(96)06028-6]

I. INTRODUCTION

Manganese-based oxide perovskites, $RE_{1-x}AE_xMnO_3$ (where RE is a trivalent rare-earth ion and AE a divalent ion such as Ca, Sr, Ba, or Pb), have long been known to exhibit a phase transition to a ferromagnetic metallic (FM) state at the Curie temperature T_C.[1–5] Recent studies for thin films,[6–11] ceramics,[12,13] and single crystals with finely controlled compositions of these compounds[14–19] have also revealed enormous magnetoresistance (MR) phenomena: A fairly large negative MR effect is commonly observed around T_C, and in some cases an insulator-metal (I-M) transition associated with a resistivity change of over ten orders of magnitude is induced by an external magnetic field at low temperatures (the so-called colossal MR effect).[17] Origins of such a remarkable MR effect and field-induced I-M transition are the subject of current intensive studies.[20,21]

Among a number of perovskite-type manganese oxides with various combinations of (RE,AE), $La_{1-x}Sr_xMnO_3$ is considered to be a prototypical and reference material. The parent compound $LaMnO_3$ is an antiferromagnetic correlated insulator (Mott insulator) with a Néel temperature $T_N \sim 140$ K (the A-type spin structure[22,23]). The Mn^{3+} ion has an electronic configuration of $3d^4 : t_{2g}^3 e_g^1$. Charge carriers are doped by substitution of La^{3+} with Sr^{2+} ions into the Mn e_g orbitals that are strongly hybridized with O $2p$ orbitals. These carriers become itinerant through the network of the MnO_6 octahedra, and simultaneously can mediate the ferromagnetic kinetic exchange interaction (the so-called double-exchange interaction) between the localized Mn t_{2g} spins (the spin quantum number $S = 3/2$). A distinct feature is that the spins of both t_{2g} and e_g electrons tend to align parallel on the Mn site because the intra-atomic exchange interaction [Hund's-rule coupling $J_H \approx 1.2$ eV (Ref. 24)] between

these spins is sufficiently large compared with the transfer interaction t of the e_g electrons between the neighboring Mn sites.

For $La_{1-x}Sr_xMnO_3$ crystals, the FM state appears below T_C and above a critical composition of $x_c \approx 0.17$ (compositional I-M phase boundary), and develops up to $T_C \approx 380$ K at the doping level of $x = 0.3$–0.5.[14,15] The large reduction in resistivity upon the thermally induced FM phase transition and the large negative MR phenomena observed around T_C are ascribed mostly to the same origin: The alignment of the local t_{2g} spins upon the FM phase transition or by applying a magnetic field considerably reduces the spin-disorder scattering of the conduction e_g carriers and hence the resistivity. It has been revealed experimentally that the thermally induced and the field-induced resistivity changes have a similar scaling behavior as a function of the spontaneous magnetization and the field-induced magnetization, respectively. Furukawa[20] showed that these behaviors can be quantitatively explained in terms of the double-exchange model,

$$H = -t \sum_{i,j,\sigma} (c_{i\sigma}^\dagger c_{j\sigma} + \text{h.c.}) - J_H \sum_i \vec{\sigma}_i \cdot \vec{S}_i. \quad (1)$$

Here the first term represents the hopping process of the e_g carriers and the second term the Hund's-rule coupling between the spin of the e_g carrier ($\vec{\sigma}_i$) and the localized t_{2g} spin ($\vec{S}_i$) on the same Mn site.

In addition to the electronic properties resulting from the strong spin-charge coupling as described above, the distorted perovskite lattice of $La_{1-x}Sr_xMnO_3$ undergoes a structural phase transition[25,26] between a low-temperature orthorhombic form [$Pnma$(No. 62):$Z = 4$, hereafter referred to as the O phase] and a high temperature rhombohedral one [$R\bar{3}c$(No. 167):$Z = 2$, R phase] as a function of the compo-
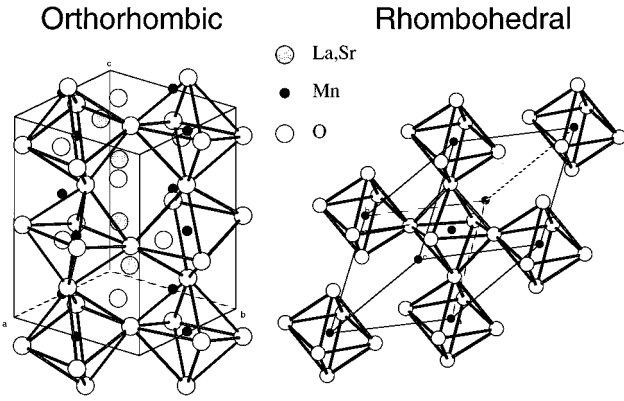
Orthorhombic   Rhombohedral

- ◎ La,Sr
- ● Mn
- ○ O

FIG. 1. Schematic crystal structures of $La_{1-x}Sr_xMnO_3$ in a low temperature orthorhombic (O) phase and in a high temperature rhombohedral (R) one. The lattice parameters for the $x=0.170$ crystal are summarized in Table I.

sition x, temperature, and/or pressure. These crystal structures are depicted schematically in Fig. 1. The change of the crystal structure can also couple to the transport properties of the system. In such a slightly distorted perovskite-type structure, a MnO_6 octahedron is alternately rotated and tilted along the pseudocubic axes, so that the Mn-O-Mn bond angle is deviated from the ideal case of 180°. This buckling of the MnO_6 octahedra reduces the transfer interaction t of the e_g carriers and hence increases the resistivity. This fact is well known for the e_g carrier-based conductors, which shows up most dramatically in the I-M phenomena of the $RENiO_3$ perovskites[27] depending on the variation of the buckling that is sensitive to the ionic radius of the RE ion. In the case of $La_{1-x}Sr_xMnO_3$, the transfer interaction of the e_g carriers is expected to be larger in the R phase than in the O phase. Thus not only the local spins but also the lattice distortion strongly couples with the charge dynamics in $La_{1-x}Sr_xMnO_3$ crystals.

In this paper we describe interesting magnetostructural phenomena that result from the mutual coupling among the t_{2g} local-spin moments, the kinetic energy of doped e_g carriers, and the lattice distortion. We have investigated thermally induced and field-induced structural phase transitions for $La_{1-x}Sr_xMnO_3$ crystals with finely controlled carrier densities ($x=0.160$, 0.170, and 0.180). For the crystal with an optimized composition ($x=0.170$), which is tuned so that the structural transition temperature T_S is located slightly above T_C (≈ 264 K) at zero field, the T_S is decreased drastically from 280 K at zero field down to 220 K at 7 T. Utilizing the structural phase diagram determined in the plane of temperature and magnetic field, we can switch the crystal structure reversibly and irreversibly between the O and R phases by an application of magnetic field. On the other hand, the structural phase transition has been less de-

pendent on magnetic fields for $x=0.16$ or 0.18 crystals, since their T_S and T_C differ considerably, either $T_S \gg T_C$ or $T_S \ll T_C$, and hence the effective coupling between the magnetization and the lattice distortion is reduced.

Part of the results for the $x=0.170$ crystal has been published in the form of a short paper.[28] Here we present a systematic study of field-induced structural phase transitions with changes of x and temperature together with an analysis in terms of Landau theory for the coupled order parameter transition. In Sec. II we describe the details of the crystal preparation and the x-ray structural analysis. Experimental procedures for measurements of the resistivity and the lattice striction as a function of temperature and magnetic field are presented. Experimental results are presented in Sec. III. In Sec. IV we discuss the thermodynamical aspects of the magnetostructural phenomena semiquantitatively in terms of the free-energy consideration as a function of the magnetization and the lattice distortion. Section V is devoted to a summary of the present study.

II. CRYSTAL PREPARATION AND EXPERIMENTAL PROCEDURE

All crystals of $La_{1-x}Sr_xMnO_3$ ($x=0.160$, 0.170, and 0.180) were melt-grown by a floating-zone method, as published previously in Refs. 15 and 29. The starting materials, La_2O_3, $SrCO_3$, and Mn_3O_4, were mixed with the prescribed ratio and calcined three times in air at 1050 °C for 24 h with intermittent grinding. Then the obtained powder was pressed into a rod with a size of 5 mm$\phi \times$60 mm and sintered in air at 1350 °C for 24 h. Crystal growth was carried out in a flow of air with a floating-zone furnace equipped with two halogen incandescent lamps. The feeding speed is 5–10 mm/h. More detailed conditions for the crystal growth are found in the above references.

To characterize the crystals, powder x-ray-diffraction measurement and electron probe microanalysis were carried out. The analyses indicated that all the crystals are homogeneous and of single phase. A four-circle x-ray-diffraction measurement was also performed, but it was difficult to determine the details of the crystal structure such as the Mn-O-Mn bond angle or the atomic coordinates, because the crystals seem to suffer from multidomain structures upon the structural phase transition. The crystallographic data obtained from the analyses are summarized in Table I.

In order to confirm the thermally induced structural phase transition between the O and R phases as well as its hysteretic nature, the change of the orthorhombic (022) peak intensity with temperature was traced in zero field, as shown in Fig. 2 for the $x=0.170$ crystal. The inset indicates the position of the peak in the O phase. The structural transition in the temperature (T) sweep shows a hysteresis with a width of about 10 K. In the temperature-decreasing run, an over-

TABLE I. Crystallographic data for the $x=0.170$ crystal determined from the x-ray powder diffraction.

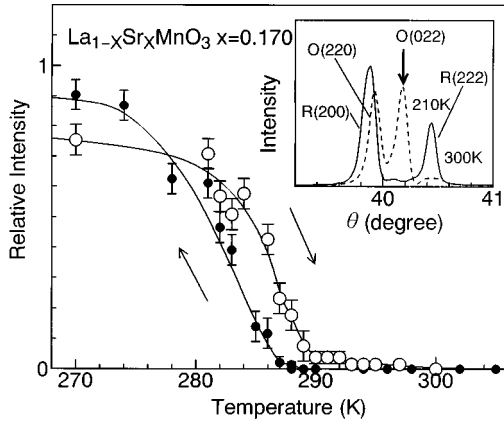| Crystal system	Space group	Lattice parameters (Å)	Volume (Å^3/Mn site)
Rhombohedral (290 K)	$R\bar{3}c$(No. 167)	$a=5.475(1)$, $\alpha=60.997°$	59.290(3)
Orthorhombic (280 K)	$Pnma$(No. 62)	$a=5.547(1)$, $b=7.790(1)$, $c=5.502(1)$	59.445(3)

FIG. 2. Temperature dependence of the orthorhombic (022) peak intensity in $La_{1-x}Sr_xMnO_3$ ($x=0.170$) determined by the measurement of x-ray powder diffraction pattern. The arrows indicate the direction of the temperature sweep. The inset shows some diffraction peaks for the rhombohedral (R, a solid line) and orthorhombic (O, a broken line) phases.

shooting behavior in the intensity is observed, which is gradually extinguished with a further lowering of temperature. This overshooting behavior often seems to be seen in quantities relating to the lattice transformation (e.g., in the striction), which probably reflects the first-order nature of this transition.

The structural as well as its electronic phase diagram[15] of $La_{1-x}Sr_xMnO_3$ crystal with the composition x as an abscissa is shown in Fig. 3. It is to be noted that the structural transition temperature T_S sharply decreases with increasing x, e.g., from $T_S \approx 325$ K at $x=0.160$ down to 160 K at $x=0.180$, while the Curie temperature T_C rises from 250 up to 292 K, respectively. Thus, the fine control of the composition in a step of $\delta x=0.005$ is required to optimize the field-switching characteristics of the crystal structure.

For simultaneous measurements of the resistivity and the lattice striction, the crystal was cut to a rectangular shape
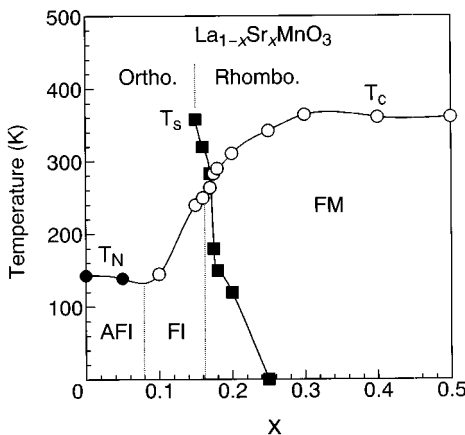

FIG. 3. Structural as well as electronic phase diagram of $La_{1-x}Sr_xMnO_3$ with the composition x. T_S, T_N, and T_C stand for structural, antiferromagnetic, and ferromagnetic transition temperatures, respectively. The abbreviations mean antiferromagnetic insulator (AFI), ferromagnetic insulator (FI), and ferromagnetic metal (FM).
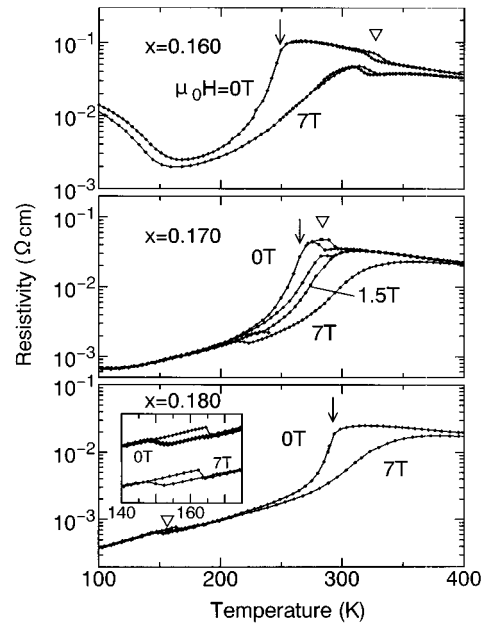

FIG. 4. Temperature dependence of resistivity in $La_{1-x}Sr_xMnO_3$ with $x=0.160$, 0.170, and 0.180 in magnetic fields. The arrows indicate the Curie temperature T_C and the triangles the structural phase transition between the O and R phases. The inset of the bottom panel ($x=0.180$) shows a magnification (arbitrarily offset in an ordinate scale) of the transition region.

with typical dimensions of 7 mm in length, 3 mm in width, and 0.7 mm in height. Such a fairly large surface area is needed to minimize the errors in the striction measurement. The resistivity was measured along the length employing the conventional four-point probe method. Heat-treatment-type silver paint (heated at 550 °C for 30 min) was used for the electrodes. The striction was measured using a uniaxial strain gauge (Kyowa Electronic Instrument Co., Ltd.) attached to the other side of the crystal. The striction was monitored as a resistance change of the gauge ($\delta R/R$, where R is the resistance of the gauge), and was deduced by the relation $\delta L/L = K^{-1} \delta R/R$ (L is the length and $K \approx 2$ the gauge factor). The resolution of $\delta L/L$ was about 1×10^{-6}.

III. RESULTS

A. Resistivity anomalies due to the structural transitions

Figure 4 shows the temperature dependence of the resistivity ρ for $x=0.160$, 0.170, and 0.180 crystals in various magnetic fields. In zero field, the hysteretic behaviors in ρ are seen upon the structural phase transition with decreasing and increasing temperature, as indicated by a triangle. The Curie temperature T_C is indicated by an arrow. In addition to the large negative MR effect around T_C, the R-to-O structural phase-transition point tends to be lowered with an application of a magnetic field but in quite an x-dependent manner. For example, the decrease in T_S at 7 T is about 9 and 4 K for $x=0.160$ and 0.180, respectively, while for $x=0.170$ it is as large as 55 K. It is worth noting that the difference between T_S and T_C at zero field is only about 20 K for the $x=0.170$, while $T_S - T_C \approx 75$ K and -140 K for $x=0.160$ and 0.180. These results suggest that such a gigan-
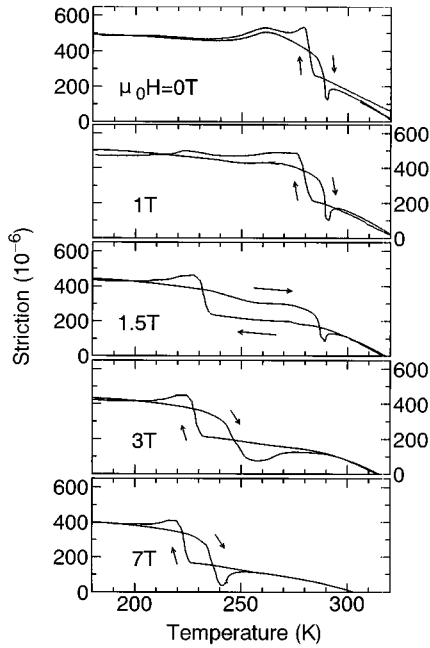
FIG. 5. Temperature dependence of the striction at various magnetic fields in $La_{1-x}Sr_xMnO_3$ ($x=0.170$). The arrows indicate the direction of the temperature sweep.

tic magnetostructural effect observed for the $x=0.170$ crystal is closely related to the large negative MR effect around T_S. For the $x=0.170$ crystal, the hysteresis loop expands across T_C over the temperature range of 50 K at 1.5 T. At a high field (7 T) the loop appears below T_C. These behaviors will be discussed in Sec. IV in terms of the coupled order parameters in the Landau free energy. Hereafter, we focus mainly on the experimental results for the $x=0.170$ crystal.

B. Structural phase diagram for $x=0.170$: temperature sweep

In Fig. 5 we show the temperature dependence of the striction ($\delta L/L$) for the $x=0.170$ crystal at various magnetic fields. Arrows indicate the direction of the T sweep. Corresponding to the structural phase transition, the striction changes abruptly by $200-400\times 10^{-6}$. The behaviors of the striction, namely, the transition temperatures and the hysteresis, correspond to those of the x-ray Bragg reflection peak shown in Fig. 2 in zero field, and also to those of the resistivity under magnetic fields shown in Fig. 4. Thus we can determine the R-O transition temperatures under a magnetic field by measurements of the striction as well as of the resistivity.

Figure 6 shows the structural phase diagrams in the plane of temperature and magnetic field for $x=0.160$, 0.170, and 0.180 crystals, which were obtained from the results in the T-sweep runs. The structural transition temperatures from the R-to-O phase in the temperature-decreasing run are shown by closed symbols, and open ones indicate the reverse transformation in the temperature-increasing run. The region surrounded with the two-phase boundary lines is the hysteretic region where both the O and R structures can be realized as temperature is increased or decreased. As the magnetic field is increased, T_S for $x=0.170$ sharply decreases around
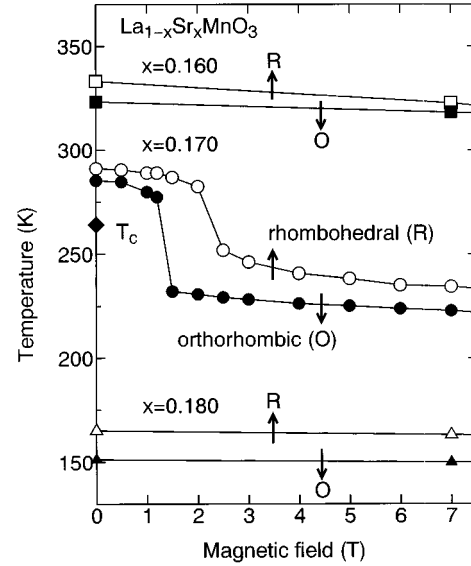

FIG. 6. Magnetostructural phase diagrams obtained from the T-sweep experiments at a constant field for $x=0.160$, 0.170, and 0.180. The open and closed symbols stand for the transitions from the O to the R phase and the reverse transition, respectively. The region surrounded by the two phase boundaries is a hysteretic region.

1.5 T across T_C, and then becomes less field dependent, while for $x=0.160$ or 0.180 it does not change conspicuously up to 7 T.

C. Structural phase diagram for $x=0.170$: field sweep

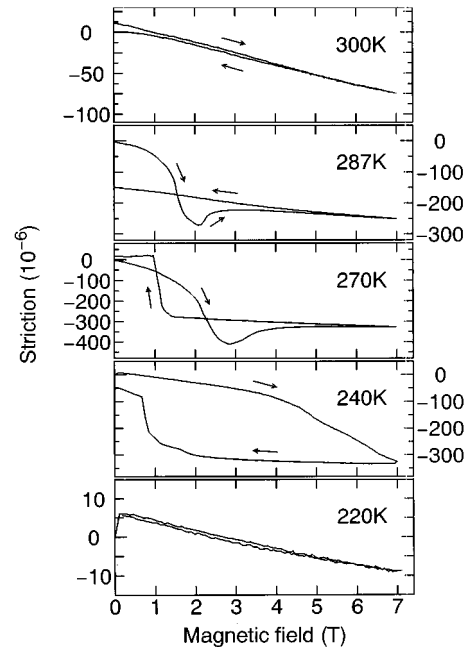Figure 7 shows the magnetic-field dependence of the striction for the $x=0.170$ crystal at various temperatures. The

FIG. 7. Magnetic-field dependence of striction at various temperatures in $La_{1-x}Sr_xMnO_3$ ($x=0.170$). The arrows indicate the direction of the H sweep. At $T=240$, 270, and 287 K, a structural phase transition is induced by a magnetic field (see text).
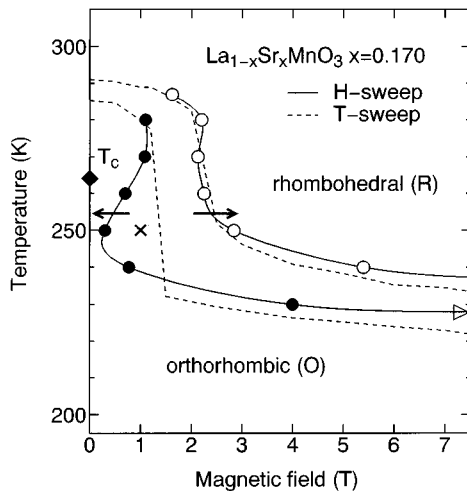
FIG. 8. Magnetostructural phase diagram for $x=0.170$ obtained from the H-sweep experiments of Fig. 7. For a comparison, the dotted lines show the phase boundaries of Fig. 6, which are obtained in the T-sweep runs. The results clearly demonstrate that the crystal structure is path dependent in the H-T plane (see text).

crystal structure before the field (H) sweep is orthorhombic for $T=220$, 240, 270, and 287 K, and rhombohedral for $T=300$ K (see also Fig. 6). As for the case of $T=287$ K, the temperature is within the hysteretic region, and the crystal was first cooled below 200 K at zero field and then warmed to 287 K so that the crystal is in the O phase.

At $T=220$ and 300 K, the striction shows a gradual change with field, but no clear sign for the first-order field-induced structural phase transition. However, a fairly large striction induced by a magnetic field indicates the presence of strong coupling between the magnetization and the lattice striction which is inherent to the present crystal. Incidentally, a steep change of the striction observed below 0.1 T at 220 K is perhaps due to the conventional magnetostriction relevant to the domain-wall motion in the ferromagnetic phase. At $T=240$, 270, and 287 K, on the other hand, a steep change of the striction with magnetic field was observed, perhaps corresponding to the O-R structural phase transitions induced by a magnetic field. For example, the transition at $T=240$ and 270 K is thermodynamically reversible between the O and R phases, while at $T=287$ K it is irreversible from the O-to-R phase.

The structural phase diagram is shown in Fig. 8, which was obtained from the above results in the H-sweep runs. The dotted lines are the phase boundaries obtained for the case of T-sweep runs shown in Fig. 6. These phase diagrams are nearly identical, but discrepancies are seen in the temperature region between 240 and 270 K: The hysteretic field region is more expanded in the H-sweep runs than in the T-sweep ones. In the latter case (dotted lines), the phase boundaries show a steep change at the same region. These results clearly demonstrate that the structural phase in this crystal is path dependent in the field-temperature plane. The main cause of the difference of the first-order transition lines is the effect of thermal fluctuations. In the case of the H-sweep runs, the thermal energy at a local potential minimum of the free energy does not change throughout the experiment, while in the case of the T-sweep ones the thermal

energy itself changes. For example, let us consider a point (1 T, 250 K) in the field-temperature phase diagram in Fig. 8 (marked with $\times$). At this point, the O structure is thermodynamically stable. In the T-sweep runs, The R-to-O transition readily occurs at a higher temperature around 280 K, and hence the crystal remains the O phase when the temperature is decreased to 250 K under a constant field of 1 T. On the other hand, the field-induced R phase undergoes supercooling due to the reduced thermal fluctuations, when the field is decreased to 1 T at a constant temperature of 250 K. Thus the hysteretic field region tends to expand, as seen in Fig. 8, with a decrease of temperature from 280 to 250 K.

IV. DISCUSSION

As is well known, the Zeeman energy of an electron spin in a magnetic field is estimated as 0.7 K/T per a Bohr magneton μ_B. We first discuss qualitatively the reason why such a small perturbation as a magnetic field can trigger the enormous magnetostructural effect observed in $La_{1-x}Sr_xMnO_3$ ($x=0.170$).

In general, a magnetic material placed in an external magnetic field H gains its free energy mainly by the Zeeman term, $-MH$, and hence prefers a high-M state. In the case of the $La_{1-x}Sr_xMnO_3$ crystal, the transfer interaction of e_g carriers that is responsible for the ferromagnetic double-exchange interaction and hence the induced magnetization M are larger in the R phase than in the O phase. Therefore, the crystal tends to be more stabilized in the R phase than in the O phase in a magnetic field. This expectation is in accord with the observed structural phase diagrams of Figs. 6 and 8, where the R phase is extended in a wide temperature region under a magnetic field.

Figure 9 shows some plots of free energy as a function of two order parameters, the magnetization M and the lattice distortion Q, which is calculated using Eq. (2) (see below). Before going to the details of the free-energy calculation, let us briefly discuss the qualitative aspects of the free-energy change under a magnetic field. Here we simplify the difference in the lattice structures of the O and R phases in terms of a single order parameter Q; a small Q value (≈ 0) stands for the R phase and a large Q value (≈ 1) for the O phase. The figure represents a structural phase transition induced by a magnetic field from the O-to-R phase at a fixed temperature ($=270$ K). In zero field above T_C (e.g., at 270 or 287 K in Fig. 7), let us assume that the O phase with a larger Q value is thermodynamically stable. The situation is represented in the upper two panels of Fig. 9; that is, the minimum of the free energy is located at $M=0$ and $Q\approx 1$. Then the magnetization M appears in both phases with an increase of the magnetic field. As described above, the gain of the free energy is expected to be larger in the R phase than in the O phase, since the double-exchange interaction is more effective in the R phase and hence a larger M appears. The lower two panels of Fig. 9 clearly show that the minimum of the free energy has moved to a point with a higher M value and $Q\approx 0$, which means that the O-to-R structural transition has been completed. Thus it is possible to trigger a structural phase transition by a magnetic field. From the above arguments, it is likely that such an effect is pronounced when the field-induced magnetization differs in both phases whose
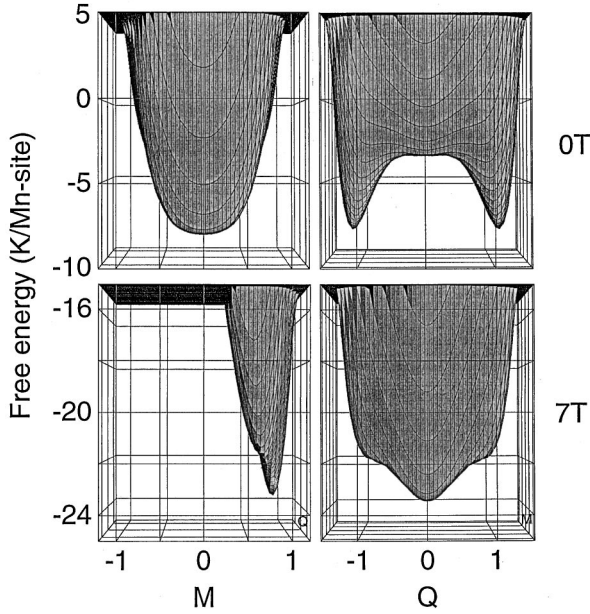
FIG. 9. Perspectives of free energy at 270 K (immediately above $T_C = 264$ K) for La$_{1-x}$Sr$_x$MnO$_3$ ($x = 0.170$) as a function of two order parameters, the magnetization M and the lattice distortion Q, which is calculated using Eq. (2) with fitted parameters (see text). The upper two panels show the free energy in zero field and the lower two panels in 7 T. The figure represents a structural phase transition induced by a magnetic field from an orthorhombic ($Q \approx 1$) to a rhombohedral ($Q \approx 0$) phase at a fixed temperature.

free energies are nearly degenerate in zero field. Therefore, it is necessary to tune the composition x so finely that T_S and T_C are close as in the case of La$_{1-x}$Sr$_x$MnO$_3$ ($x = 0.170$).

In order to elucidate such a coupled phenomenon between M and Q semiquantitatively, we calculated a magnetostructural phase diagram in terms of the Landau free-energy expansion with the coupled order prameters,[30,31]

$$f = f_0 + \frac{A(T - T_C^0)}{2} M^2 + \frac{T_\beta}{4} M^4 - MH + \frac{A'(T - T_S^0)}{2} Q^2$$

$$- \frac{T'_\beta}{4} Q^4 + \frac{T'_\gamma}{6} Q^6 + \frac{T_\eta}{2} M^2 Q^2, \qquad (2)$$

where f_0 is a constant part of the free energy, A, T_β, A', T'_β, T'_γ, and T_η are parameters, and T_C^0 ($= 282$ K) and T_S^0 ($= 285.3$ K) denote the Curie temperature in the R phase[32] and the R-to-O structural transition temperature in the temperature-decreasing run under zero field, respectively. Note that the observed T_C (≈ 264 K) at zero field is for the O phase, and hence reduced from T_C^0 due to the lattice distortion. The first line was adopted for the ferromagnetic phase transition of the second order, the second for the structural phase transition of the first order, and the last for the coupling between M and Q. The parameters could be determined from the experiment: for example, the Curie constant of the susceptibility above T_C gives A, and the hysteretic width of the structural transition at zero field of Fig. 2, the steep decrease in the structural transition temperature of Fig. 6, and the temperature difference of the Curie point in the O and R phases[32] set an appropriate range of the other pa-
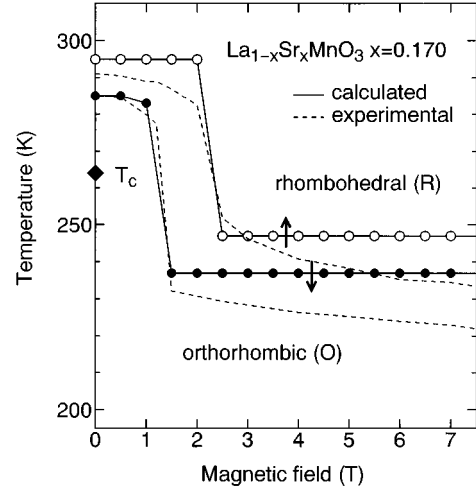

FIG. 10. Magnetostructural phase diagram calculated using the free energy with coupled order parameters, the magnetization M and the lattice distortion Q [Eq. (2)]. The dotted lines are the experimentally observed phase boundaries of Fig. 6.

rameters. The dimensionless order parameters M and Q were normalized appropriately at each transition point.

Figure 10 shows a calculated magnetostructural phase diagram in La$_{1-x}$Sr$_x$MnO$_3$ ($x = 0.170$) using Eq. (2). In a unit of f with K/Mn site, the Zeeman term is fixed as $-2.7MH$ (T) where we assumed the spin moment of $4\mu_B$/Mn site. The parameters are $A = 3$, $T_\beta = 95$ K, $A' = 0.665$, $T'_\beta = T'_\gamma = 26.8$ K, and $T_\eta = 32$ K, which were adjusted but only in a limited range in order to best reproduce the phase diagram of Fig. 6. The free-energy functions as depicted in Fig. 9 examplify the calculated results with use of these parameters at 270 K and at fields of 0 (upper panel) and 7 T (lower panel). Within an approximation neglecting the effect of thermal fluctuations, we can determine the phase diagram by taking the transition points where the height of the potential barrier becomes zero. We confirmed that the calculations employing T- or H-sweep method gives an identical phase diagram with a neglect of the thermal fluctuations. The calculation is in fairly good agreement with the experimental results. However, we note several problems, apart from its oversimplified modeling, in this calculation: First the calculation cannot correctly reproduce the temperature dependence of M in La$_{1-x}$Sr$_x$MnO$_3$ ($x = 0.170$) below T_C. The critical exponent of M ($\propto |T - T_c|^{2\beta}$) is $\beta = 0.25$ in this model, while a recent neutron-diffraction study for La$_{1-x}$Sr$_x$MnO$_3$ ($x = 0.3$) (Ref. 33) has revealed that $\beta = 0.295$. The saturation to $M = 1$ appears to be singular, which is the reason why the transition points are field independent in a high-field region as seen in the figure. Second, the calculated transition temperatures tend to be a little higher than the experimental ones. This is probably due to an ignorance of thermal fluctuations.

Finally we comment on the relation between the magnetostructural phenomena in the present study and the possible structural effect in large negative MR phenomena in La$_{1-x}$Sr$_x$MnO$_3$. Although it has been shown in the present study that the lattice degree of freedom is in fact correlated with the charge degree of freedom and hence with the magnetism as described above, we would like to emphasize that

this is a rather special case when the coupling is much pronounced by tuning the composition so finely such that T_S and T_C nearly coincide. As suggested from the electronic phase diagram of Fig. 3, the structural transition and the ferromagnetic transition in $La_{1-x}Sr_xMnO_3$ are essentially independent. It should be noticed, however, that the above argument does not necessarily mean to exclude the possibility that the large negative MR phenomena as well as the ferromagnetic transition in this compound is related to a change of the lattice form such as a distortion of MnO_6 octahedra or a dynamical Jahn-Teller effect,[21] because the measurement of the lattice striction adopted in the present study can only detect a static structural effect.

On the other hand, a number of recent experimental studies in the related compounds, e.g., $(La_{1-y}Pr_y)_{0.7}Ca_{0.3}MnO_3$,[13] $Pr_{1-x}Sr_xMnO_3$,[16] $Pr_{1-x}Ca_xMnO_3$,[17] and $(Nd_{1-y}Sm_y)_{1/2}Sr_{1/2}MnO_3$,[18,19] have shown clearly that hysteretic behaviors show up in the field-induced I-M transition, or colossal MR effect and the ferromagnetic transition. These observations suggest (and have already confirmed) that the field-induced structural changes are accompanied by the transitions. In these compounds with a narrower bandwidth than $La_{1-x}Sr_xMnO_3$, we consider that the charge-ordering (CO) instability of doped carriers plays an important role, which can drag, more or less, the additional lattice distortion. In $La_{1-x}Sr_xMnO_3$ crystals, however, the CO instability has not yet been observed in the presently focusing range of the composition.

V. SUMMARY

We have investigated magnetic-field-induced structural phase transitions as well as thermally induced ones for perovskite-type manganese oxides, $La_{1-x}Sr_xMnO_3$, with finely controlled composition (x=0.160, 0.170, and 0.180). In an x=0.170 crystal, the composition is tuned so that the structural transition temperature is close to the ferromagnetic transition temperature T_C. As a result, interesting magneto-structural phenomena have been observed: the rhombohedral-orthorhombic transition temperature is lowered by more than 50 K with the application of an external magnetic field of a few T. For x=0.160 or 0.180 crystals, on the other hand, such a large effect has not been found up to 7 T although the change (several K) of the structural transition temperature was observed under a magnetic field of several T. We have determined the structural phase diagram for the x=0.170 crystal in the plane of temperature and magnetic field from the measurement of the lattice striction by T-sweep as well as H-sweep runs. It has been revealed that such a large magnetostructural effect arises from the mutual coupling among the kinetic energy of e_g carriers, t_{2g} local-spin moments, and lattice distortion. Thermodynamical aspects of the magnetostructural phenomena have been discussed in terms of the free energy with coupled order parameters, the magnetization, and the lattice distortion, which can explain the observed results semiquantitatively.

[1] G. H. Jonker and J. H. Van Santen, Physica **16**, 337 (1950); G. H. Jonker, *ibid.* **22**, 707 (1956).

[2] C. Zener, Phys. Rev. **82**, 403 (1951).

[3] P. W. Anderson and H. Hasegawa, Phys. Rev. **100**, 675 (1955).

[4] P.-G. de Gennes, Phys. Rev. **118**, 141 (1960).

[5] K. Kubo and N. Ohata, J. Phys. Soc. Jpn. **33**, 21 (1972).

[6] C. W. Searle and S. T. Wang, Can. J. Phys. **47**, 2703 (1969).

[7] R. M. Kusters, D. A. Singleton, R. Mcgreevy, and W. Hayes, Physica B **155**, 362 (1989).

[8] K. Chahara, T. Ohno, M. Kasai, and Y. Kozono, Appl. Phys. Lett. **63**, 1990 (1993).

[9] R. von Helmont, J. Wecker, B. Holzapfel, M. Schultz, and K. Samwer, Phys. Rev. Lett. **71**, 2331 (1993).

[10] S. Jin, T. H. Tiefel, M. McCormack, R. Fastnacht, R. Ramesh, and L. H. Chen, Science **264**, 413 (1994).

[11] G. C. Xiong, Q. Li, H. L. Ju, S. N. Moo, L. Senapati, X. X. Xi, R. L. Greene, and T. Venkatesan, Appl. Phys. Lett. **66**, 1427 (1995).

[12] B. Raveau, A. Maignan, and B. Caignaert, J. Solid State Chem. **117**, 424 (1995).

[13] H. Y. Hwang, S.-W. Cheong, P. G. Radaelli, M. Marezio, and B. Batlogg, Phys. Rev. Lett. **75**, 914 (1995).

[14] Y. Tokura, A. Urushibara, Y. Moritomo, T. Arima, A. Asamitsu, G. Kido, and N. Furukawa, J. Phys. Soc. Jpn. **63**, 3931 (1994).

[15] A. Urushibara, Y. Moritomo, T. Arima, A. Asamitsu, G. Kido, and Y. Tokura, Phys. Rev. B **51**, 11 103 (1995).

[16] Y. Tomioka, A. Asamitsu, Y. Moritomo, H. Kuwahara, and Y. Tokura, Phys. Rev. Lett. **74**, 5108 (1995).

[17] Y. Tomioka, A. Asamitsu, Y. Moritomo, and Y. Tokura, J. Phys. Soc. Jpn. **64**, 3626 (1995).

[18] H. Kuwahara, Y. Tomioka, A. Asamitsu, Y. Moritomo, and Y. Tokura, Science **270**, 961 (1995).

[19] H. Kuwahara, Y. Tomioka, Y. Moritomo, A. Asamitsu, M. Kasai, and Y. Tokura, Science **272**, 80 (1996).

[20] N. Furukawa, J. Phys. Soc. Jpn. **63**, 3214 (1994).

[21] A. J. Millis, P. B. Littlewood, and B. I. Shraiman, Phys. Rev. Lett. **74**, 5144 (1995); A. J. Millis, B. I. Shraiman, and R. Mueller (unpublished).

[22] E. O. Wollan and W. C. Koehler, Phys. Rev. **100**, 545 (1955).

[23] J. B. Goodenough, Phys. Rev. **100**, 564 (1955).

[24] Y. Okimoto, T. Katsufuji, T. Ishikawa, A. Urushibara, T. Arima, and Y. Tokura, Phys. Rev. Lett. **75**, 109 (1995).

[25] A. Wold and R. J. Arnott, J. Phys. Chem. Solids **9**, 176 (1959).

[26] J. B. Goodenough and J. M. Long, in *Magnetic and Other Properties of Oxides and Related Compounds*, edited by K.-H. Hellwege and A. M. Hellwege, Landolt-Börnstein, New Series Group III, Vol. 4, Pt. a (Springer, Berlin 1970).

[27] J. B. Torrance, P. Lacorre, A. I. Nazzal, E. J. Ansaldo, and Ch.

Niedermayer, Phys. Rev. B **45**, 8209 (1992).

[28] A. Asamitsu, Y. Moritomo, Y. Tomioka, T. Arima, and Y. Tokura, Nature (London) **373**, 407 (1995).

[29] Y. Moritomo, A. Asamitsu, and Y. Tokura, Phys. Rev. B **51**, 16 491 (1995).

[30] E. M. Lifshiz and L. P. Pitaevskii, in *Statistical Physics*, edited by L. D. Landau and E. M. Lifshitz, Course of Theoretical Physics Vol. 3 (Pergamon, Oxford, 1978), Chap. 14.

[31] Y. Imry, J. Phys. C **8**, 567 (1975).

[32] A structural phase diagram in the plane of temperature and pressure can be obtained from the measurement of the resistivity under a pressure, which nearly scales with the magnetostructural phase diagram presented in this study. In this case, we can determine T_C's by measuring ac susceptibilities under a pressure both in the O and R phases: Y. Moritomo, A. Asamitsu, and Y. Tokura (unpublished).

[33] M. C. Martin, G. Sirane, Y. Endoh, K. Hirota, Y. Tokura, and Y. Moritomo, Phys. Rev. B **53**, 14 285 (1996).